

# High-resolution chemical imaging of gold nanoparticles using hard x-ray ptychography

**Hoppe, R.; Reinhardt, J.; Hofmann, G.; Patommel, J.; Grunwaldt, J.-D.; Damsgaard, Christian Danvad; Wellenreuther, G.; Falkenberg, G.; Schroer, C. G.**

*Published in:*
Applied Physics Letters

*Link to article, DOI:*
10.1063/1.4807020

*Publication date:*
2013

*Document Version*
Publisher's PDF, also known as Version of record

AIP | Applied Physics Letters

# High-resolution chemical imaging of gold nanoparticles using hard x-ray ptychography

R. Hoppe, J. Reinhardt, G. Hofmann, J. Patommel, J.-D. Grunwaldt et al.

Citation: Appl. Phys. Lett. **102**, 203104 (2013); doi: 10.1063/1.4807020
View online: http://dx.doi.org/10.1063/1.4807020
View Table of Contents: http://apl.aip.org/resource/1/APPLAB/v102/i20
Published by the AIP Publishing LLC.

# High-resolution chemical imaging of gold nanoparticles using hard x-ray ptychography

R. Hoppe,[1] J. Reinhardt,[1,4,a)] G. Hofmann,[2] J. Patommel,[1] J.-D. Grunwaldt,[2] C. D. Damsgaard,[3] G. Wellenreuther,[4] G. Falkenberg,[4] and C. G. Schroer[1]
[1]*Institute of Structural Physics, Technische Universität Dresden, D-01062 Dresden, Germany*
[2]*Institute for Chemical Technology and Polymer Chemistry, Karlsruhe Institute of Technology, D-76131 Karlsruhe, Germany*
[3]*Center for Electron Nanoscopy and Department of Physics, Technical University of Denmark, DK-2800 Lyngby, Denmark*
[4]*Deutsches Elektronen-Synchrotron DESY, D-22607 Hamburg, Germany*

(Received 17 November 2012; accepted 27 April 2013; published online 20 May 2013)

We combine resonant scattering with (ptychographic) scanning coherent diffraction microscopy to determine the chemical state of gold nanoparticles with high spatial resolution. Ptychographic images of the sample are recorded for a series of energies around the gold $L_3$ absorption edge. From these data, chemical information in the form of absorption and resonant scattering spectra is reconstructed at each location in the sample. For gold nanoparticles of about 100 nm diameter, a spatial resolution of about 20–30 nm is obtained. In the future, this microscopy approach will open the way to operando studies of heterogeneous catalysts on the nanometer scale. © *2013 AIP Publishing LLC*.
[http://dx.doi.org/10.1063/1.4807020]

Catalysts play a key role in chemical industry, energy-related processes, and exhaust gas after-treatment. Nowadays, almost all chemicals are produced using at least one catalytic step. In order to optimize catalytic processes, for example, in view of catalyst activity, selectivity, or lifetime, it is crucial to understand the function of the catalyst under realistic working conditions.[1] This requires monitoring the chemical state of the catalyst on a large range of length scales, from the atomic level up to the size of the catalytic reactor.[2] X-ray microscopy is an ideal technique to address this question, in particular with the chemical sensitivity obtained with x-ray absorption spectroscopy as contrast.[3] The greatest advantage of x-ray microscopy over other techniques is that hard x-rays can penetrate the chemical reactor and thus allow the investigation of catalysts in operando.[4] In combination with tomographic techniques, even the local chemical state inside the sample can be reconstructed.[5]

Conventional x-ray microscopy is limited in spatial resolution, covering the length scales above several tens of nanometers. The resolution gap between conventional microscopy and the atomic level can be bridged by coherent x-ray diffraction imaging techniques.[6] In particular, scanning coherent x-ray diffraction microscopy, also known as ptychography,[7] can overcome the limits of conventional x-ray microscopy in terms of spatial resolution and at the same time image extended objects.[8,9] The method has quickly found applications[10,11] and has been extended to three dimensions by a combination with tomography.[11,12] In addition, ptychography can be combined with spectroscopic techniques. This has been demonstrated in the soft x-ray range[13] discriminating between micrometer sized spheres of different materials by evaluating the attenuation and phase shift at a few energies around the oxygen K edge. Recently, by a differential contrast measurement at the gold $L_3$ edge, it was possible to discriminate between gold and silver at high spatial resolution in Au/Ag nanoparticles.[14]

In this letter we used resonant spectroscopic ptychography to image the local chemical state of gold nanoparticles with high spatial resolution (20–30 nm), obtaining full resonant scattering spectra around the $L_3$ edge of gold at each location in the image. In this way, chemical information can be gained for single nanoparticles and with unprecedented sensitivity, i.e., for about $16 \times 10^6$ atoms in a gold nanoparticle (27 attomol). This is important for studying *in situ* catalytic reactions, in particular on the scale of single catalytic nanoparticles.

The experiment was carried out at the nanoprobe endstation at beamline P06 of the synchrotron radiation source PETRA III at DESY in Hamburg, Germany.[15] This hard x-ray scanning microscope is well suited for ptychographic imaging at high spatial resolution, optimizing the x-ray intensity on the sample by scanning the sample locally with an intense nanofocused beam.[9,16] The synchrotron radiation beam from the undulator source is monochromatized by a Si (111) double-crystal monochromator. In the hard x-ray scanning microscope located about 98 m from the source, the beam is focused by a pair of nanofocusing refractive x-ray lenses made of silicon.[17] For this particular experiment at the gold $L_3$ edge, a hard x-ray nanobeam with full-width-at-half-maximum (FWHM) lateral dimensions of $130 \times 230\,\text{nm}^2$ (vertical × horizontal) was used to record the ptychographic datasets of a test sample.

This sample made of gold nanoparticles on a silicon nitride membrane was prepared by drop coating a suspension of 100 nm gold colloids in water (from BBI) onto a TEM sample grid with a 20 nm thick silicon nitride membrane (from TEMwindows.com). The shape of the particles is mostly spherical-like (>95 %), but uneven shapes (<5 %), e.g., triangular ones, are also present. After drying, the sample was inspected by an FEI Helios EBS3 dual-beam

a)Electronic mail: reinhardt@xray-lens.de

 

electron microscope mounted with a gas injection system (GIS) and precursor ($C_9H_{16}Pt$) that enables electron beam induced deposition (EBID) of platinum. Interesting areas were marked by a platinum ring with a diameter of 1 $\mu$m and a width and thickness of approximately 100 nm. Fig. 1(a) shows a scanning electron microscopy (SEM) image of the sample. After inspection, the sample was coated with approximately 5 nm of carbon to avoid static charging in the x-ray beam.

Of this sample, we acquired two series of ptychographic datasets around the Au $L_3$ absorption edge. Each ptychographic dataset contains 441 far-field diffraction patterns acquired by scanning a total field of view of $1 \times 1\ \mu m^2$ in $20 \times 20$ steps of 50 nm step size. The diffraction patterns were recorded by a Pilatus 300 k (Ref. 18) pixel detector located 2 m downstream of the sample position. The first dataset comprises ptychograms every 5 eV from 11896 eV to 11946 eV with an exposure time of 1.5 s per scan point. The second set is composed of ptychograms recorded in intervals of 1 eV in the energy range from 11912 eV to 11921 eV and with an exposure time of 0.3 s per scan point. The acquisition of a dataset with 1.5 s exposure time per scan point took less than 15 min, one with 0.3 s exposure time about 3 min. From each ptychographic dataset the complex transmission function (attenuation and phase shift) of the object is reconstructed together with the complex wave field of the illuminating beam.[19,20]

Figs. 1(b) and 1(c) show the ptychographic reconstruction of the nanoparticles in modulus and phase, respectively. For gold nanoparticles of this size, the signal-to-noise ratio in the phase is much better than in the modulus (maximal attenuation: 1.4%). Quantitatively, a maximal phase shift of about $-100$ mrad is measured, in good agreement with that expected for 100 nm of gold.

Similar reconstructions are obtained for all energies. From the reconstructed data, the modulus and phase at each position in the object can be extracted as a function of energy. In this way, the change in phase shift due to resonant scattering and that in modulus due to absorption can be extracted locally.

Fig. 2(b) shows the phase as function of energy for several nanoparticles marked in Fig. 2(d). The other gold particles marked in red in Fig. 2(e) show similar spectra. The phase inside rectangle A on the platinum ring [Fig. 2(d)] exhibits a flat spectrum apart from fluctuations. The phase inside rectangle B in Fig. 2(d) on the $Si_3N_4$ membrane served as reference. The refraction and thus the (negative) phase shift by the gold particle are reduced as a consequence of resonant scattering at the $L_3$ absorption edge of gold. This is quite a strong effect, reducing the refractive power by about one quarter. The aim is to determine the local chemical environment of the given atomic species (gold), e.g., its oxidation state. This can be done by comparing the measured data to reference spectra.

The solid and the dashed curves show the resonant spectrum in the phase for metallic and trivalent gold, respectively,

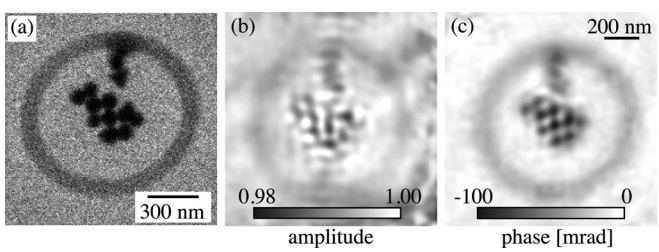


FIG. 1. (a) SEM image of 100 nm Au nanoparticles framed by a platinum ring. The modulus (b) and phase shift (c) of the object as reconstructed from the ptychogram recorded with an exposure time of 1.5 s at 11896 eV.

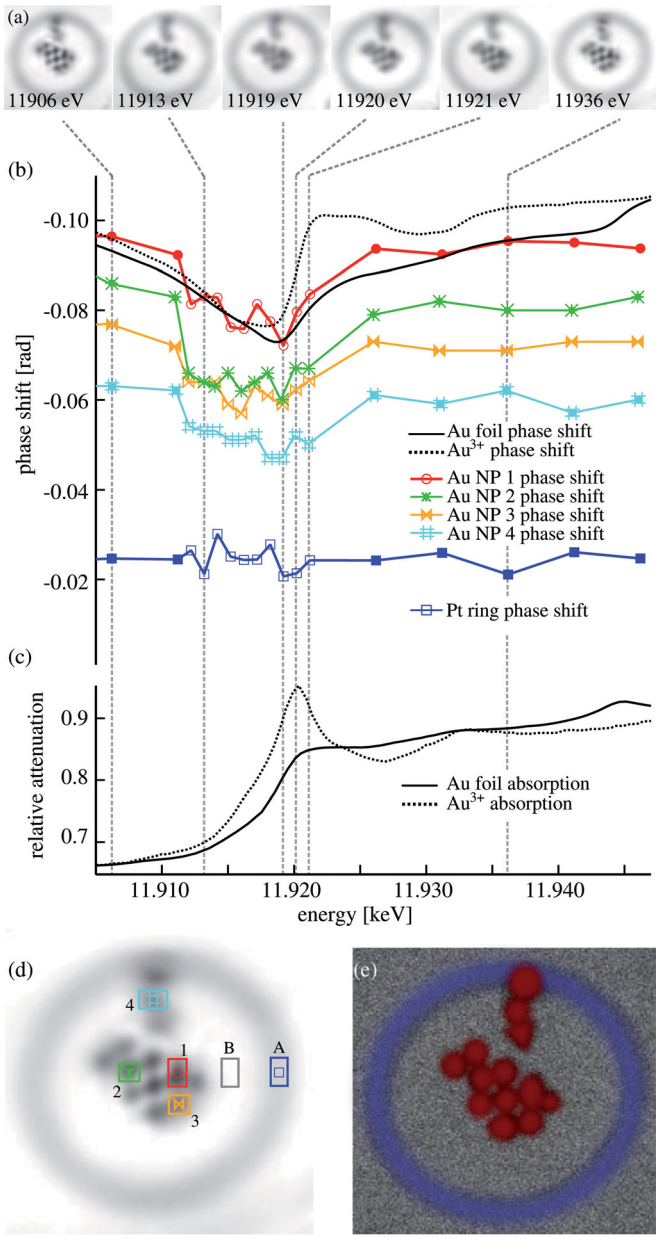


FIG. 2. (a) ptychographic reconstruction of the phase shift of the object at selected energies [same grey scale as in Fig. 1(c)]. (b) Phase shift of different gold nanoparticles marked in Fig. 2(d) as function of x-ray energy, showing a reduced refraction at the gold $L_3$ edge. Full and open markers correspond to 1.5 s and 0.3 s exposure time per scan point, respectively. The phase shift of the platinum ring inside rectangle A in Fig. 2(d) shows no significant energy dependence in the range around the $L_3$ edge of gold (full and open squares). The fluctuations in the platinum signal may be regarded as the error level for the reconstructed phase. (c) As reference, the absorption of a metallic gold foil (solid curve) and trivalent gold ($HAuCl_4$ in aqueous solution, dashed curve) is shown. By using the Kramers-Kronig relation the phase shift of the metallic gold foil (solid) and of trivalent gold (dashed) were calculated and are shown in (b). Fig. 2(e) visualizes the elemental distribution in the sample, red areas are gold and blue area is platinum.

as calculated using the Kramers-Kronig relation[21] from absorption spectra of the two chemical species shown in Fig. 2(c). The spectra of the four selected particles [Fig. 2(d)] are well matched by that of the metallic gold foil [cf., Fig. 2(b)]. A contribution of trivalent gold lies below the noise level. Therefore, within the uncertainty introduced by the fluctuations in the spectra, these particles are in the metallic state, and the concentration of oxidized gold within the particles lies below the current detection limit. There is no oxidized gold particle in the sample. In order to improve the detection limit, the noise level in the ptychograms needs to be reduced. Currently, the fluctuations of the phase lie in the range of several milliradiants. In the future, the noise level is expected to be pushed well below the milliradiant range (cf., discussion below).

Fig. 2(a) shows the ptychographic reconstructions at selected energies [dashed vertical lines in Fig. 2(b)]. The four images right at the absorption edge (11913 eV, 11919 eV, 11920 eV, and 11921 eV) were recorded with 0.3 s exposure time and thus have a slightly reduced spatial resolution compared to the other reconstructions that were recorded with 1.5 s exposure time. In the image sequence the reduction of the phase shift is clearly visible in the gold particles, while the phase shift in the platinum ring remains unchanged. At the same time, a meaningful spectrum for the attenuation could not be extracted for these small particles as the signal-to-noise ratio is not sufficient in this case.

To evaluate the spatial resolution in the ptychograms, we compare the reconstructions with model calculations. From the SEM image [cf., Fig. 3(a)], a transmission model is constructed of perfect gold spheres shown in Fig. 3(b). This idealized transmission model is convolved with a Gaussian blur to match quantitatively the phase distribution in the reconstructed images. We used the width of the Gaussian blur (FWHM) as the only fit parameter. Figs. 3(c) and 3(d) show the reconstruction and the best fit by the model image, respectively, for the case of an exposure time of 1.5 s, yielding a spatial resolution of about 19 nm (FWHM). For the shorter exposure time of 0.3 s, the comparison shown in Figs. 3(e) and 3(f) yields a spatial resolution of about 27 nm (FWHM).

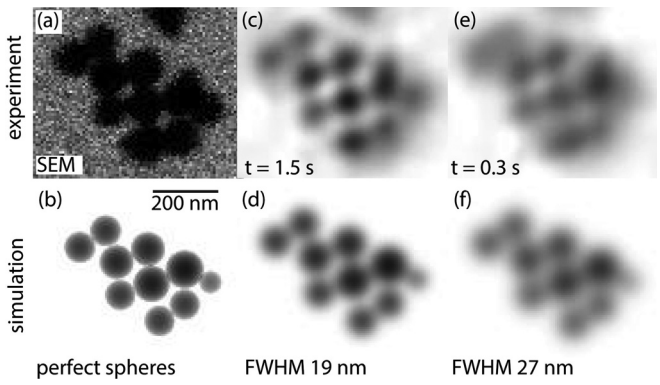


FIG. 3. (a) SEM image of the central part of the test sample [cf., Fig. 1(a)], (b) arrangement of model gold nanoparticles. (c) Reconstructed object with an exposure time of 1.5 s per scan point, (d) model object with a Gaussian blur of about 19 nm (FWHM). (e) Reconstruction of a dataset with short exposure time (0.3 s), best modeled by a Gaussian blur of 27 nm (FWHM) shown in (f).

The spatial resolution of a ptychographic reconstruction depends on the statistics in the diffraction patterns.[9,16] The resolution of the reconstructions with the longer exposure times, i.e., 1.5 s, is about 1.4 times higher than that of those with the shorter exposure time (0.3 s). This is in good agreement with the difference in resolution expected for diffraction from a generic object, i.e., a factor $\sqrt[4]{5} \approx 1.5$ for diffraction patterns that follow an approximate power law behavior of $q^{-4}$ with increasing momentum transfer $q$.[22]

In order to improve the spatial resolution in the future, the fluence[23] on the sample needs to be increased. This can be achieved by increasing both the exposure time and the coherent flux density on the sample. At beamline P06 at PETRA III, the latter can be achieved by focusing the coherent flux to the aperture of the nanofocusing optic.[15] In this way, the fluence can be increased by at least three orders of magnitude compared to the current experiment, leading to an increase in spatial resolution by almost one order of magnitude. A spatial resolution of a few nanometers should be achievable for small metallic particles. As the detectability of a feature, e.g., a catalytic particle or part of it, is nearly independent of its surrounding,[16] it should be possible to investigate supported catalysts inside a micro reactor with high imaging quality in the future.

For such weakly scattering objects, such as these small catalytic nanoparticles, background scattering from the flight-tube window in front of the detector, the air gap between flight tube and detector, and the detector itself can be quite significant compared to the diffraction signal from the sample. Here, we subtracted the background using a model based on elastic and Compton scattering prior to ptychographic reconstruction. For even more weakly scattering samples and for higher spatial resolution, this background needs to be reduced in the future, e.g., by placing the detector in vacuum or using an appropriate data acquisition procedure with beam stops.

Resonant scanning coherent diffraction imaging has significant advantages over conventional x-ray scanning microscopy, e.g., with transmission or fluorescence contrast. Besides the intrinsically enhanced spatial resolution, chromatic effects in the nanofocusing optic are fully compensated. For instance, the refractive x-ray optics used in this experiment are chromatic, i.e., the focal length changes with energy. Thus the illumination in the sample plane changes slightly from energy to energy, affecting the spatial resolution in conventional scanning microscopy, like micro x-ray absorption near edge structure (XANES) spectroscopy in absorption and fluorescence mode. The ptychographic reconstruction, however, automatically compensates for chromatic changes as long as the defocused illumination in the sample plane is not excessively large. The spatial resolution is unaffected, independent of the chromaticity of the optics. In addition, the technique yields the resonant scattering signal that has a significantly better signal-to-noise ratio than the attenuation for small objects. Therefore, it is ideally suited to image mesoscopic catalytic particles. In the next step, we will investigate catalytic nanoparticles in operando.

The authors thank P. Bhargava, N. Reimers, B. de Samber (DESY), D. Samberg (TU Dresden), A. Fuller, and J. B. Wagner (DTU) for their technical support. This work

was supported by the German Ministry of Education and Research (BMBF) under Grant Nos. 05K10OD1 and 05K10VK1 and by VH-VI-403 of the Impuls- und Vernetzungsfonds (IVF) of the Helmholtz Association of German Research Centres. G.H. was supported by the Helmholtz-Kolleg "Energy Related Catalysis." Beamtime at beamline P06 at PETRA III was granted within the in-house program of DESY. Gold references were measured at beamline microXAS at synchrotron radiation source SLS at PSI.

[1]H. Topsøe, J. Catal. **216**, 155 (2003); B. M. Weckhuysen, Chem. Commun. **2002**, 97 (2002); J.-D. Grunwaldt and B. S. Clausen, Top. Catal. **18**, 37 (2002).
[2]A. T. Bell, Science **299**, 1688 (2003); J.-D. Grunwaldt, J. B. Wagner, and R. E. Dunin-Borkowski, Chem. Cat. Chem. **5**, 62 (2013); B. M. Weckhuysen, Angew. Chem., Int. Ed. **48**, 4910 (2009); A. Urakawa and A. Baiker, Top. Catal. **52**, 1312 (2009).
[3]J.-D. Grunwaldt and C. G. Schroer, Chem. Soc. Rev. **39**, 4741 (2010).
[4]J.-D. Grunwaldt, S. Hannemann, C. G. Schroer, and A. Baiker, J. Phys. Chem. B **110**, 8674 (2006); S. Hannemann, J.-D. Grunwaldt, N. van Vegten, A. Baiker, P. Boye, and C. G. Schroer, Catal. Today **126**, 54 (2007); J.-D. Grunwaldt, B. Kimmerle, A. Baiker, P. Boye, C. G. Schroer, P. Glatzel, C. N. Borca, and F. Beckmann, *ibid.* **145**, 267 (2009); S. Hannemann, J.-D. Grunwaldt, B. Kimmerle, A. Baiker, P. Boye, and C. Schroer, Top. Catal. **52**, 1360 (2009).
[5]C. G. Schroer, M. Kuhlmann, T. F. Günzler, B. Lengeler, M. Richwin, B. Griesebock, D. Lützenkirchen-Hecht, R. Frahm, E. Ziegler, A. Mashayekhi, D. Haeffner, J.-D. Grunwaldt, and A. Baiker, Appl. Phys. Lett. **82**, 3360 (2003).
[6]J. Miao, P. Charalambous, J. Kirz, and D. Sayre, Nature (London) **400**, 342 (1999); C. G. Schroer, P. Boye, J. Feldkamp, J. Patommel, A. Schropp, A. Schwab, S. Stephan, M. Burghammer, S. Schöder, and C. Riekel, Phys. Rev. Lett. **101**, 090801 (2008); Y. Takahashi, Y. Nishino, R. Tsutsumi, H. Kubo, H. Furukawa, H. Mimura, S. Matsuyama, N. Zettsu, E. Matsubara, T. Ishikawa, and K. Yamauchi, Phys. Rev. B **80**, 054103 (2009).
[7]J. M. Rodenburg and H. M. L. Faulkner, Appl. Phys. Lett. **85**, 4795 (2004); P. Thibault, M. Dierolf, A. Menzel, O. Bunk, C. David, and F. Pfeiffer, Science **321**, 379 (2008).
[8]Y. Takahashi, A. Suzuki, N. Zettsu, Y. Kohmura, Y. Senba, H. Ohashi, K. Yamauchi, and T. Ishikawa, Phys. Rev. B **83**, 214109 (2011).
[9]A. Schropp, R. Hoppe, J. Patommel, D. Samberg, F. Seiboth, S. Stephan, G. Wellenreuther, G. Falkenberg, and C. G. Schroer, Appl. Phys. Lett. **100**, 253112 (2012).
[10]K. Giewekemeyer, P. Thibault, S. Kalbfleisch, A. Beerlink, C. M. Kewish, M. Dierolf, F. Pfeiffer, and T. Salditt, Proc. Natl. Acad. Sci. U.S.A. **107**, 529 (2010); A. Schropp, P. Boye, A. Goldschmidt, S. Hönig, R. Hoppe, J. Patommel, C. Rakete, D. Samberg, S. Stephan, S. Schöder *et al.*, J. Microsc. **241**, 9 (2011).
[11]R. N. Wilke, M. Priebe, M. Bartels, K. Giewekemeyer, A. Diaz, P. Karvinen, and T. Salditt, Opt. Express **20**, 19232 (2012).
[12]M. Dierolf, A. Menzel, P. Thibault, P. Schneider, C. M. Kewish, R. Wepf, O. Bunk, and F. Pfeiffer, Nature (London) **467**, 436 (2010); A. Diaz, P. Trtik, M. Guizar-Sicairos, A. Menzel, P. Thibault, and O. Bunk, Phys. Rev. B **85**, 020104(R) (2012).
[13]M. Beckers, T. Senkbeil, T. Gorniak, M. Reese, K. Giewekemeyer, S.-C. Gleber, T. Salditt, and A. Rosenhahn, Phys. Rev. Lett. **107**, 208101 (2011).
[14]Y. Takahashi, A. Suzuki, N. Zettsu, Y. Kohmura, K. Yamauchi, and T. Ishikawa, Appl. Phys. Lett. **99**, 131905 (2011).
[15]C. G. Schroer, P. Boye, J. M. Feldkamp, J. Patommel, D. Samberg, A. Schropp, A. Schwab, S. Stephan, G. Falkenberg, G. Wellenreuther, and N. Reimers, Nucl. Instrum. Methods Phys. Res. A **616**, 93 (2010).
[16]A. Schropp and C. G. Schroer, New J. Phys. **12**, 035016 (2010).
[17]C. G. Schroer, O. Kurapova, J. Patommel, P. Boye, J. Feldkamp, B. Lengeler, M. Burghammer, C. Riekel, L. Vincze, A. van der Hart, and M. Küchler, Appl. Phys. Lett. **87**, 124103 (2005).
[18]P. Kraft, A. Bergamaschi, C. Broennimann, R. Dinapoli, E. F. Eikenberry, B. Henrich, I. Johnson, A. Mozzanica, C. M. Schlepuetz, P. R. Willmott, and B. Schmitt, J. Synchrotron Radiat. **16**, 368 (2009).
[19]A. M. Maiden and J. M. Rodenburg, Ultramicroscopy **109**, 1256 (2009).
[20]This has revolutionized the characterization of nanobeams and optics [C. M. Kewish, M. Guizar-Sicairos, C. Liu, J. Qian, B. Shi, C. Benson, A. M. Khounsary, J. Vila-Comamala, O. Bunk, J. R. Fienup *et al.*, Opt. Express **18**, 23420 (2010); C. M. Kewish, P. Thibault, M. Dierolf, O. Bunk, A. Menzel, J. Vila-Comamala, K. Jefimovs, and F. Pfeiffer, Ultramicroscopy **110**, 325 (2010); A. Schropp, P. Boye, J. M. Feldkamp, R. Hoppe, J. Patommel, D. Samberg, S. Stephan, K. Giewekemeyer, R. N. Wilke, T. Salditt *et al.*, Appl. Phys. Lett. **96**, 091102 (2010); S. Hönig, R. Hoppe, J. Patommel, A. Schropp, S. Stephan, S. Schöder, M. Burghammer, and C. G. Schroer, Opt. Express **19**, 16325 (2011); J. Vila-Comamala, A. Diaz, M. Guizar-Sicairos, A. Mantion, C. M. Kewish, A. Menzel, O. Bunk, and C. David, *ibid.* **19**, 21333 (2011)].
[21]J. Als-Nielsen, *Elements of Modern X-Ray Physics* (John Wiley & Sons, Kopenhagen, 2002).
[22]M. R. Howells, T. Beetz, H. N. Chapman, C. Cui, J. M. Holton, C. J. Jacobsen, J. Kirz, E. Lima, S. Marchesini, H. Miao, D. Sayre, D. A. Shapiro, J. C. H. Spence, and D. Starodub, J. Electron Spectrosc. **170**, 4 (2009).
[23]The fluence is the number of photons per area, with which the sample was exposed. In this experiment, the detected fluence was about 6900 ph/nm$^2$ for the 1.5 s exposures and 1700 ph/nm$^2$ for those with 0.3 s exposure.